



HAL
open science

CRDS measurements of air-broadened lines in the 1.6 μm band of $^{12}\text{CO}_2$: Line shape parameters with their temperature dependence

Didier Mondelain, Alain Campargue, H el ene Fleurbaey, Semen Vasilchenko,
Samir Kassi

► To cite this version:

Didier Mondelain, Alain Campargue, H el ene Fleurbaey, Semen Vasilchenko, Samir Kassi. CRDS measurements of air-broadened lines in the 1.6 μm band of $^{12}\text{CO}_2$: Line shape parameters with their temperature dependence. *Journal of Quantitative Spectroscopy and Radiative Transfer*, 2022, 288, pp.108267. 10.1016/j.jqsrt.2022.108267 . hal-03854989

HAL Id: hal-03854989

<https://hal.science/hal-03854989>

Submitted on 21 Nov 2022

HAL is a multi-disciplinary open access archive for the deposit and dissemination of scientific research documents, whether they are published or not. The documents may come from teaching and research institutions in France or abroad, or from public or private research centers.

L'archive ouverte pluridisciplinaire **HAL**, est destin ee au d ep ot et  a la diffusion de documents scientifiques de niveau recherche, publi es ou non,  emanant des  tablissements d'enseignement et de recherche fran ais ou  trangers, des laboratoires publics ou priv es.



Distributed under a Creative Commons Attribution 4.0 International License

1 **CRDS measurements of air-broadened lines in the 1.6 μm band of $^{12}\text{CO}_2$:**
2 **Line shape parameters with their temperature dependence**
3

4
5 D. Mondelain*, A. Campargue, H. Fleurbaey, S. Kassı, S. Vasilchenko
6

7 *Univ. Grenoble Alpes, CNRS, LIPhy, 38000 Grenoble, France*
8
9

10
11
12 *Corresponding author: didier.mondelain@univ-grenoble-alpes.fr; LIPhy, Bat. E, 140 rue de la
13 Physique, 38400 Saint-Martin d'Hères (France).
14
15
16
17
18
19
20
21

22 **Key words**

23 Line shape; carbon dioxide; temperature dependence; CRDS
24

25 **Abstract**

26 The $^{12}\text{CO}_2$ band at 1.6 μm is used for carbon dioxide monitoring in the Earth atmosphere. The
27 targeted accuracy of these measurements motivates important efforts to improve the quality of the
28 spectroscopic parameters in atmospheric conditions. In the present work, the line shapes of the R(6),
29 R(12), R(16), R(18) and R(20) transitions of the 30013-00001 band of $^{12}\text{CO}_2$ in air are studied with a
30 cavity ring down spectrometer (CRDS). For each transition, high signal-to-noise ratio spectra
31 (between 2000 and 20000) are recorded at different temperatures (250, 274, 285, 295 and 320 K)
32 and total pressures (50, 100, 250, 500 and 750 Torr). To this end, a spectrally narrowed and stable
33 (sub-kHz) laser source is coupled into a temperature regulated high-finesse optical cavity. The
34 frequency scale of each spectrum is accurately determined from measurements of the frequency of
35 the beat note between a part of the laser light and the closest tooth of a frequency comb referenced
36 to a rubidium clock. A multi-spectrum fit procedure with quadratic speed dependent Nelkin-Ghatak
37 profiles, including line-mixing effects, has been used to derive for each transition, the different
38 spectroscopic parameters and their temperature dependence. Results are discussed in comparison
39 with previous experimental data, HITRAN2020 database and values obtained from requantized
40 classical molecular dynamics simulations (rCMDS).

41

42 1. Introduction

43 Due to its importance for remote sensing applications from ground- or satellite-based
44 observatories, the 30013-00001 band of $^{12}\text{CO}_2$ in the 1.6 μm atmospheric transparency window has
45 been the subject of many laboratory studies using Fourier transform spectroscopy (FTS) [1,2 and
46 references herein] and cavity ring down spectroscopy (CRDS) [3,4,5,6,7]. This band is especially used
47 to monitor the column averaged CO_2 atmospheric dry air mole fraction, X_{CO_2} , in several satellite
48 missions like the Orbiting Carbon Observatory-2 (OCO-2) [8,9,10], OCO-3 [11] and GOSAT [12]. A
49 relative uncertainty of less than 0.3 % (*i.e.* ~ 1 ppm) is required [13] to better characterize the surface
50 CO_2 sources and sinks on regional scales and constrain the climate models. This brings strong quality
51 constraints on the spectroscopic parameters which have to be determined with very small
52 uncertainties. As stated in [14], *the spectroscopic error estimates (...) are generally comparable to or*
53 *larger than the noise-only X_{CO_2} posterior uncertainty (...)*, showing the importance of new
54 experimental data with improved accuracy. Moreover, upcoming missions like CO2M [15] will have
55 even stronger requirements on X_{CO_2} with a spectroscopic error contribution to the systematic error of
56 0.13 ppm (or 0.0325%) [16]. Here, the systematic error is interpreted as a *differential* systematic
57 error corresponding to the difference of spectroscopic error contribution between extreme
58 atmospheric states when a global bias (of 0.4 ppm) is allowed. This leads to strong constraints on the
59 spectroscopic parameters and their temperature dependence. For example, as described in [17], the
60 air broadening coefficients and their temperature dependence exponents have to be known with an
61 accuracy better than 0.1% and 0.005, respectively. In parallel, it is necessary to make available
62 accurate spectroscopic line-shape parameters for CO_2 lines to improve the semi-empirical models
63 used to update all of the carbon dioxide transitions in the spectroscopic databases (*e.g.* HITRAN [18]
64 or GEISA [19]), especially for the non-Voigt parameters [20]. The same accurate experimental data
65 are also valuable for validation tests of the parameters provided by requantized classical molecular
66 dynamics simulations (rCMDS) [21].

67 This work has been done in the frame of the project entitled *Improved Spectroscopy for Carbon*
68 *Dioxide, Oxygen, and Water Vapour Satellite Measurements* funded by the European Space Agency
69 (ESA). The aim of this work is to determine the line-shape parameters and their temperature
70 dependence with a reduced uncertainty to meet the targeted accuracies mentioned above. This is
71 done for five transitions belonging to the R-branch of the 30013-00001 band of $^{12}\text{CO}_2$ in air. These
72 data will serve as validation of Fourier transform measurements by Deutsches Zentrum für Luft- und
73 Raumfahrt (DLR) which will be available within a later work package of the ESA project. To achieve
74 this goal, parameters are retrieved from high signal-to-noise ratio CRDS spectra recorded at different
75 temperature and pressure conditions with a spectrally narrowed and stable (sub-kHz) laser source
76 coupled into a temperature regulated high-finesse optical cavity. The frequency scale of each

77 spectrum is accurately determined from measurements of the frequency of the beat note between a
78 part of the laser light and the closest tooth of a frequency comb referenced to a rubidium clock. The
79 experimental set-up is described in Part 2 together with the recording procedure. The multi-
80 spectrum fit procedure and the retrieved spectroscopic parameters are detailed in Part 3. The latter
81 are compared with the most recent and accurate experimental and theoretical data in Part 4 before
82 concluding (Part 5).
83

84 2. Experimental details

85 2.1 The setup

86 The comb-referenced cavity ring down spectrometer used for the recordings has been detailed in
87 [22] and is only briefly described here. The light source consists in a distributed feedback (DFB) laser
88 diode narrowed to sub-kHz level thanks to an optical feedback signal from a stable V-shape high
89 finesse cavity (FSR= 480 MHz; finesse= 500000) made of ultra-low expansion glass [23]. At the same
90 time, the optical feedback allows locking the laser diode to one of the longitudinal cavity modes. The
91 continuous tuning of the light source is achieved thanks to a Mach-Zehnder modulator (MZM)
92 generating a side-band scanned between 2 GHz and 22 GHz from the carrier frequency (*i.e.* over 0.67
93 cm^{-1}). By locking the laser diode to different cavity modes and changing the side band frequency, a
94 continuous tuning is achieved between 6231.5 cm^{-1} and 6243.5 cm^{-1} with the DFB diode at disposal
95 (From Fitel). Due to the low efficiency ($\sim 5\%$) of the MZM, the output beam is amplified by a booster
96 optical amplifier (BOA) before being separated in three parts: towards the high finesse cavity, the
97 wavelength meter (HighFinesse WSU7-IR) and the frequency comb (Model FC 1500-250 WG from
98 Menlo Systems).

99 Most of the light is coupled into a temperature stabilized high finesse cavity (TS-HFC) described in
100 [24] where ring down (RD) events are achieved at resonance by switching the laser light off with an
101 acousto-optic modulator (AOM). The extinction coefficient, $\alpha(\nu)$, is deduced from:

$$102 \quad \alpha(\nu) = \frac{n}{c\tau(\nu)} - \frac{1}{c\tau_0(\nu)} \quad (1)$$

103 where τ and τ_0 are the RD times for the cell filled with the gas mixture and evacuated, respectively, c
104 is the speed of light and n is the refractive index of the absorbing gas. RD events are acquired at a
105 typical rate of 200 RD/s by applying a triangular voltage ramp coupled to a RD tracking loop on the
106 PZT tube on which the output cavity mirror is mounted [22].

107 Accurate measurement of the absolute frequency of the laser source is deduced at each RD event
108 from the frequency of the beat note, f_{BN} , between a part of the light source and one tooth of a
109 frequency comb (FC) [22]. The comb tooth number is determined from the wavelength meter
110 measurements.

111 Two versions of the TS-HFC, described in [22] and [24], are used here, namely the V1 (FSR= 258
112 MHz; $F \sim 211600$) and the improved V2 (FSR= 332 MHz; $F \sim 310600$) versions. Both work on the same
113 principle (see Fig.1 of Ref. [24]): a fluid, whose temperature is regulated using an external
114 refrigerated/heating circulator (model Corio 1000F from Julabo), flows through two counter-
115 propagating copper coils wrapped around a tube containing the two dielectric mirrors of the cavity.
116 An inner copper tube is placed between the mirrors to limit the convection and reduce exchange of
117 the gas inside the tube with the surrounding gas. It has been shown that the surrounded gas is very

118 well thermalized to the tube temperature (with a difference smaller than 0.05°C) [22]. The latter is
 119 measured by four 3-wires 1000 Ω platinum temperature sensors (⅓ DIN class B; accuracy: ±0.1 K to
 120 0.2 K) for the V1 cell and by five 4-wires 100 Ω platinum temperature sensors (class 1/10 DIN) giving
 121 an accuracy equal to 0.03+0.0005t (with t the temperature in °C) for the V2 cell. In both versions, the
 122 gas temperature can be regulated over the 245-330 K range, with a maximal temperature variation
 123 along the inner tube, ΔT, of 0.5 K and 0.1 K for the for the V1 and V2 cell, respectively. The former
 124 one was used for spectra recordings at room temperature and 274 K, where ΔT is kept below 0.3 K,
 125 and the latter one at 320, 285 and 250 K (**Table 1**). The temperature variations are limited to only
 126 0.04 K over ~14h at 250 K.

127 A gas mixture of 398.9±2.0 (2σ) mol-ppm of CO₂ in air (Ar: ~1 mol-% ; O₂: ~20.95 mol-%; N₂: ~
 128 78.05 mol-%) provided by AirLiquide is used in this work. The pressure in the cells is measured by a
 129 temperature controlled absolute Baratron capacitance manometer (1000 mbar full scale; accuracy:
 130 0.10% of reading).

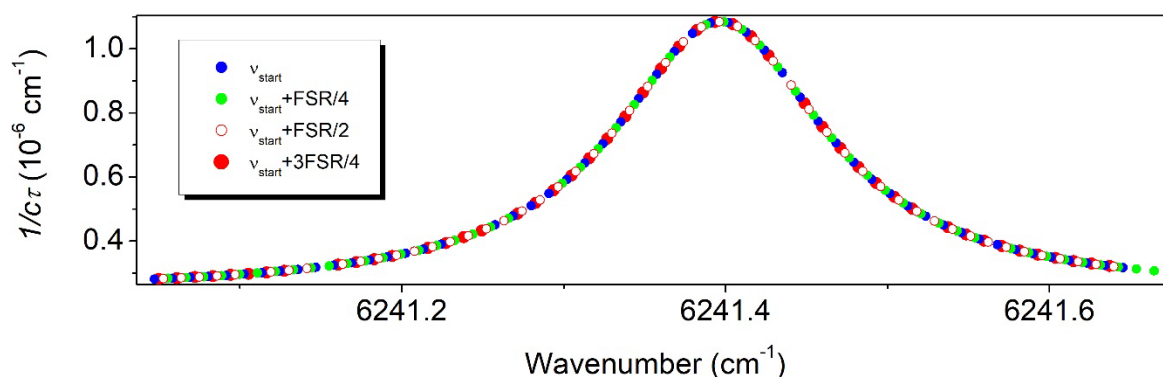
30013-00001	ν_0 cm ⁻¹	$S(296\text{ K})$ cm/mol	320K	295K	285K	274K	250K
R(6)	6233.183	1.097×10 ⁻²³	V2	V1	V2	V1	V2
R(12)	6237.421	1.656×10 ⁻²³	V2	V1	V2	V1	V2
R(16)	6240.104	1.751×10 ⁻²³	V2	V1	V2	V1	V2
R(18)	6241.403	1.721×10 ⁻²³	V2	V1	V2	V1	V2
R(20)	6242.672	1.646×10 ⁻²³	V2	V1	V2	V1	V2

131
 132 *Table 1. Summary of the temperature conditions and cell version used to record the five CO₂ transitions studied*
 133 *in this work. Position and intensity values are those provided in the HITRAN database [18].*

134
 135 **2.2. Spectra acquisition**

136 For each transition and temperature conditions reported in **Table 1**, a series of spectra are
 137 recorded for five total pressure values (750, 500, 250, 100 and 50 Torr). With the V1 cell, one
 138 spectrum was recorded for each pressure with a sampling step corresponding to the FSR of the cavity
 139 (*i.e.* 0.0087 cm⁻¹). The spectral sampling corresponding to the FSR of the cavity is adopted to increase
 140 the efficiency of the RD tracking loop (reducing the acquisition time) as the resonance always occurs
 141 at the same offset value of the ramp. With V2, the recording procedure was modified to provide
 142 more measurement points: at each pressure, four spectra were recorded for the absorption line from
 143 the starting frequency, f_{start} , for the first one and from f_{start} shifted by ¼, ½ and ¾ of the FSR value for
 144 the others (**Figure 1**). The acquisition time of one spectrum is typically 1 to 2 minutes. It is important
 145 to mention that as the CO₂ concentration can slightly evolve with time due to adsorption or
 146 desorption on the walls of the cell, it is a better choice to not concatenate the spectra recorded at a
 147 given pressure but fit them separately during the multi-spectrum fitting procedure described below.

148 In this way, the evolution of the concentration over one spectrum can be considered as negligible
 149 (0.1% in the worst case). Note that the adsorption or desorption rate depends on the temperature
 150 and pressure conditions.



151
 152 *Figure 1. The spectral sampling applied during the spectra recordings with V2 of the TS-HFC illustrated here*
 153 *for the R(18) transition at 750 Torr and 250 K with the CO₂ in air mixture. The different colors correspond to the*
 154 *four interlaced spectra.*

155 During the spectra recordings, an adaptative averaging procedure is applied to compensate the
 156 noise level increase occurring at strong absorption near the center of the lines. This involves
 157 automatically increasing the number of RDs averaged per spectral point with absorption until a user
 158 defined maximum value (in order to avoid too long acquisition times). Typically, 50 and 250 RD
 159 events are averaged in the wings and at the top of the absorption line, respectively.

160 3. Line profile analysis

161 3.1. The multi-spectrum fit procedure

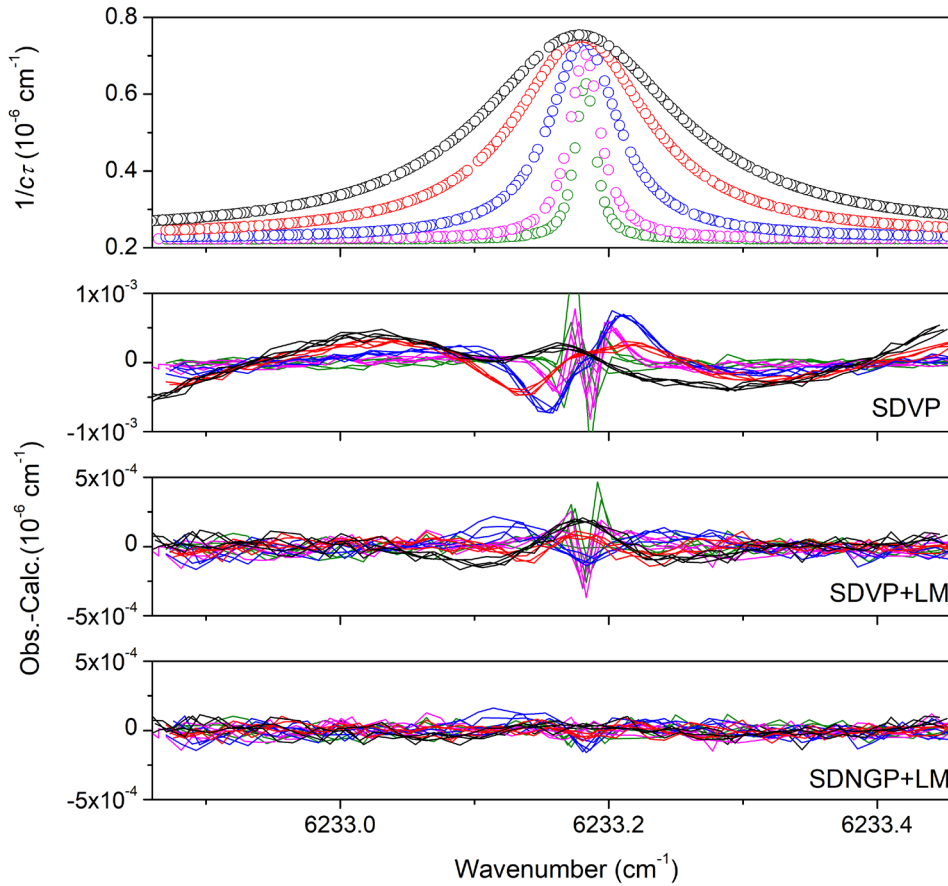
162 The same fit procedure is adopted for all the transitions: at a given temperature the five (V1 cell)
 163 or twenty spectra (corresponding to the four interlaced spectra times the five pressures in the case
 164 of the V2 cell) are taken into account in a multi-spectrum fit procedure using the *Multi-spectrum*
 165 *Analysis Tool for Spectroscopy (MATS)* fitting program [25] developed at NIST. As illustrated in **Figure**
 166 **2**, large residuals are obtained if the speed dependent Voigt profile is used. A better spectra
 167 reproduction is achieved by adding line-mixing effects but to reduce residuals to the noise level, it is
 168 necessary to use a speed-dependent Nelkin-Ghatak profile (SDNGP) [26] including first-order line
 169 mixing [27]. Note that the first-order approximation adopted in our work is valid if the off-diagonal
 170 relaxation matrix element coefficients times the pressure is much smaller than the difference
 171 between the positions of the neighbor lines [20]. This condition is verified in our case with matrix
 172 element coefficients smaller than 0.025 cm⁻¹atm⁻¹ [1] and differences in position on the order of ~1.3
 173 cm⁻¹ and maximum pressure values of 1 atm. The SDNG profile takes into account the Doppler effect,
 174 the collision-induced velocity changes, quantified by the velocity changing collision rate (in cm⁻¹), v_{VC} ,

175 the collisional broadening and shift for which a quadratic law is used for the speed dependence such
 176 that:

$$177 \quad \Gamma(\nu) = \Gamma_0 + \Gamma_2 \left[\left(\frac{\nu}{\tilde{\nu}} \right)^2 - 3/2 \right] \quad (2)$$

$$178 \quad \text{and} \quad \Delta(\nu) = \Delta_0 + \Delta_2 \left[\left(\frac{\nu}{\tilde{\nu}} \right)^2 - 3/2 \right] \quad (3)$$

179 where Γ_0 and Δ_0 (in cm^{-1}) correspond to the (thermally averaged) line width and shift, respectively,
 180 and Γ_2 and Δ_2 (in cm^{-1}) are the speed dependence components. $\tilde{\nu} = \sqrt{\frac{2k_B T}{m}}$ is the most probable
 181 speed of the absorbing molecule ($^{12}\text{C}^{16}\text{O}_2$) of mass m . The first-order line mixing is characterized by
 182 the dimensionless Y parameter (see Eq. IV.22 of [28]). Note that when fitting the correlation
 183 parameter, η , with a Hartmann Tran profile (HTP), the retrieved value is close to 0 and does not
 184 improve the fit quality. Thus, to avoid the risk of a overfitting of the spectra [29], we decided to fix η
 185 to 0 corresponding to a SDNG profile.



186
 187 *Figure 2. Series of CRDS spectra recorded for the R(6) transition at 250 K for five pressures between 50 and*
 188 *750 Torr (upper panel). Corresponding fit residuals (exp-fit) obtained after the multi-spectrum fit procedure with*
 189 *different line profiles are shown on the lower panels. The different colors correspond to the different pressures.*
 190 *For each pressure value, the residuals of the four interlaced spectra are displayed. The quality factors vary*

191 between 7700 and 14300 according to the spectrum in the case of SDNGP+LM. Note the different y-scales on
192 the residuals.

193 In the multi-spectrum fit procedure, the wavenumber of the spectral line at zero pressure, ν_0 , the
194 line-broadening and pressure-shift coefficients γ_0 (Γ_0/P , in $\text{cm}^{-1}\text{atm}^{-1}$) and δ_0 (Δ_0/P , in $\text{cm}^{-1}\text{atm}^{-1}$), their
195 speed dependence components γ_2 (Γ_2/P , in $\text{cm}^{-1}\text{atm}^{-1}$) and δ_2 (Δ_2/P , in $\text{cm}^{-1}\text{atm}^{-1}$), the Dicke
196 narrowing parameter β (ν_{vc}/P , in $\text{cm}^{-1}\text{atm}^{-1}$) and the first-order line-mixing coefficient ζ (Y/P , in atm^{-1})
197 are globally fitted for each temperature. The mixing ratio of CO_2 , X_{CO_2} , is fixed to the value of 398.9
198 ppm given by the gas supplier. The Doppler width is fixed to its calculated value at the measured
199 temperature and the line intensity, S , and the linear baseline are fitted independently for each
200 spectrum. As shown on **Figure 2** for the R(6) transition at 250 K, residuals at the noise level (which is
201 typically $5 \times 10^{-11} \text{ cm}^{-1}$ in this case) are achieved using the multi-spectrum fit procedure and
202 SDNGP+LM. This leads to quality factors between 7700 and 14300 in this case (QF is defined as the
203 ratio of the absorption at the peak to the *rms* of the residuals).

204 It is important to mention that, during the fit procedure, the absorption due to the weak CO_2 lines
205 in the neighbourhood of the fitted transition is taken into account by the *MATS* program based on
206 the HITRAN2020 database [18] using a Voigt profile and $X_{\text{CO}_2}=398.9$ ppm. If significant, absorption
207 due to the interfering water vapour transitions is also calculated and included in the simulation, using
208 the same database and a concentration fixed to a value deduced from isolated H_2O lines. Water
209 vapour mixing ratios were found to be lower than 140 ppm.

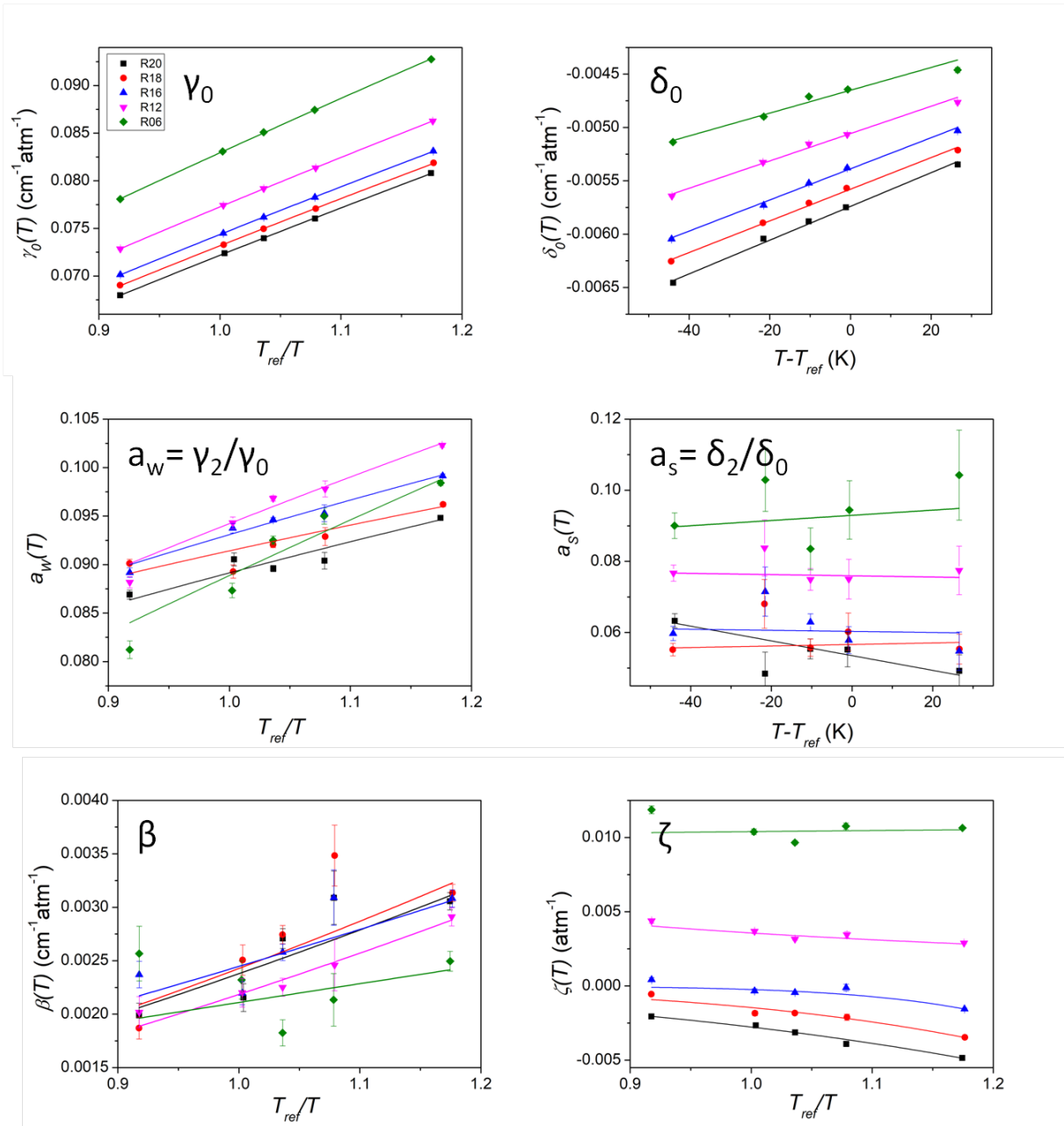
210 The parameter values of this multi-spectrum fit procedure are provided in Supplementary
211 Material for each transition at the different temperatures.

212 3.2. Temperature dependence of the line parameters

213 The multi-spectrum fit procedure applied to the five transitions provides sets of spectroscopic
214 parameters for five temperatures between 250 and 320 K. The temperature dependence of the line
215 parameters can be empirically modelled using the usual power law of the form: $A(T) =$
216 $A(T_{ref}) \left(T_{ref}/T \right)^{n_A}$ where $T_{ref} = 296$ K, $A(T)$ corresponds to either γ_0 , γ_2 , β or ζ and n_A is the
217 corresponding temperature dependence exponent. In the case of the pressure shift and its speed
218 dependence component (δ_2), the following linear dependence is applied: $\delta_i(T) = \delta_i(T_{ref}) +$
219 $\delta'_i(T - T_{ref})$ (with $i=0$ or 2) to allow for a change of sign for δ_i . Note that since we are working with
220 a mixture of CO_2 at a very low mixing ratio in air ($X_{\text{CO}_2}=398.9$ ppm), the contribution due to collisions
221 between two CO_2 molecules can be neglected for all parameters. For example, as $\gamma_0(T) =$
222 $\gamma_{self}(T)X_{\text{CO}_2}P_{tot} + \gamma_{air}(T)(1 - X_{\text{CO}_2})P_{tot}$, γ_0 can be assimilated to γ_{air} with a relative error smaller
223 than 1.5×10^{-4} .

224 Plotting the retrieved parameters $\gamma_0(T)$, $\beta(T)$ and $\zeta(T)$ versus T_{ref}/T and fitting these data points
 225 with a function of the form $y = ax^b$, allows determining $A(T_{ref})$ and n_A . In the same way, $\delta_0(T)$ is plotted
 226 versus $(T - T_{ref})$ to retrieve $\delta_0(T_{ref})$ and δ'_0 . In the case of $\gamma_2(T)$ the things are slightly different, as in the
 227 MATS program the fit output corresponds to $a_w = \frac{\gamma_2(T)}{\gamma_0(T_{ref})}$ because no temperature dependence is
 228 assumed *a priori* ($n_{\gamma_2} = 0$). Hence, by plotting $a_w(T)$ versus T_{ref}/T and fitting these data points with a
 229 function of the form $y = ax^b$ we obtain $a_w(T_{ref}) = \gamma_2(T_{ref})/\gamma_0(T_{ref})$ and n_{γ_2} . In the case of $\delta_2(T)$, the fit
 230 output corresponds to $a_s = \frac{\delta_2(T)}{\delta_0(T_{ref})}$. By plotting a_s versus $(T - T_{ref})$, we obtain $a_s(T_{ref}) = \delta_2(T_{ref})/\delta_0(T_{ref})$
 231 and δ'_2 .

232 The different parameters obtained from the multi-spectrum fit procedure are plotted versus
 233 temperature on **Figure 3**. The retrieved parameter values at T_{ref} and their temperature dependence
 234 coefficients are given in **Table 2** and compared with the most accurate literature data in the next
 235 section. Note that in the fits on **Figure 3**, the data are weighted by the inverse of the squared
 236 uncertainty estimated as discussed below.



237
 238 Figure 3. Variation of the fitted parameters of the R(6), R(12), R(16), R(18) and R(20) lines of the 30013-00001
 239 band of $^{12}\text{CO}_2$ versus the temperature. The parameters γ_0 , β , a_w , ζ are fitted with a function of the form $y = ax^b$ to
 240 determine their value at T_{ref} and the temperature dependence exponent. The δ_0 and a_s parameters are fitted
 241 with a linear function which provides their value at T_{ref} and the temperature dependence coefficient (see text).

242

	γ_0 $cm^{-1}atm^{-1}$	n_{γ_0}	δ_0 $cm^{-1}atm^{-1}$	δ' $cm^{-1}atm^{-1}K^{-1}$	θ $cm^{-1}atm^{-1}$	n_θ	a_w	n_{γ_2}	a_s^*	ζ atm^{-1}	n_ζ
R(6)	0.08295(3)	0.698(4)	-0.00465(3)	0.0000107(10)	0.00211(22)	0.8(9)	0.0889(12)	0.66(10)	0.093(5)	0.01040(49)	0.1(4)
R(12)	0.07726(1)	0.682(2)	-0.00506(2)	0.0000128(7)	0.00218(5)	1.7(2)	0.0942(6)	0.52(5)	0.076(2)	0.00357(15)	-1.4(4)
R(16)	0.07437(1)	0.683(2)	-0.00539(1)	0.0000146(5)	0.00245(10)	1.4(4)	0.0931(3)	0.39(3)	0.060(3)	-0.00024(12)	11.5(32)
R(18)	0.07318(3)	0.687(4)	-0.00558(1)	0.0000148(5)	0.00243(13)	1.8(5)	0.0914(5)	0.30(5)	0.057(2)	-0.00146(13)	5.4(6)
R(20)	0.07218(2)	0.699(3)	-0.00574(2)	0.0000158(6)	0.00238(11)	1.7(4)	0.0892(5)	0.37(4)	0.054(2)	-0.00277(6)	3.5(2)

243

244 *Note*

245 **These values correspond to the mean value averaged over all the temperatures.*

246 *Table 2. List of the spectroscopic parameters obtained for the five transitions studied in this work. A SDNG profile is used in the multi-spectrum fit procedure. One-sigma*
247 *uncertainties are given in parenthesis in the unit of the last digit. Here, a_w and a_s correspond to γ_2/γ_0 and δ_2/δ_0 , respectively.*

248 3.3 Estimated error budget

249 a. Type-A uncertainty

250 As explained in [29], the standard error provided for each fitted parameter by the MATS program
251 should be taken with caution as it could underestimate the « real error » by factors between typically
252 3 to 5, depending on the considered parameter. This is a consequence of the existence of numerical
253 correlations between the parameters which are not taken into account in the calculation of the
254 standard error. To estimate these factors in our case, we first simulated 100 spectra with different
255 random noise and then calculated the standard deviation of the fitted parameters. In our typical
256 noise conditions (10 kHz or $\sigma_x = 3 \times 10^{-3} \%$ of the Doppler FWHM on the x -axis and $1 \times 10^{-10} \text{ cm}^{-1}$ or $\sigma_y =$
257 0.02% of the maximum absorption on the y -axis), we found that the uncertainty reported for the
258 fitted parameters is equivalent to the « real error » showing that the impact of the correlation
259 between the parameters is small thanks to the low noise level on the two axis. The fit errors are thus
260 directly considered as our type-A uncertainty.

261 b. Type-B uncertainty

262 To evaluate possible biases due to inaccurate pressure and temperature values, we also adopted
263 the method described in [29] consisting, for a given transition and temperature, in: (i) generating a
264 set of spectra at the five pressures of the recordings using our list of spectroscopic parameters and a
265 SDNG profile and perturbing one parameter (the temperature or the total pressure in our case) to its
266 biased value for all the spectra and, then (ii) fitting these simulated spectra with the « true »
267 temperature or total pressure. The retrieved spectroscopic parameters are then compared to the
268 values used to generate the spectra. Here we adopted a bias of 0.1% for the total pressure,
269 corresponding to the uncertainty of the pressure gauge, and a bias of 0.1 K for the temperature
270 reflecting the uncertainty on the absolute temperature measurement and the inhomogeneity of the
271 sounded gas temperature [22]. At 274 K a bias of 0.3 K is applied due to the larger temperature
272 inhomogeneity of the V1 cell. These evaluations have been done for all the transitions and
273 temperatures. Note that a bias related to X_{CO_2} was not considered here as this parameter (in fact the
274 line intensity which is equivalent) was fitted for each spectrum. In addition, the non-linearity of the
275 acquisition board has been checked using a home-made generator of purely decreasing exponentials
276 and no effect has been noticed at the noise level of the 16 bits-acquisition board.

277 Final uncertainties on the spectroscopic parameters retrieved from the multi-spectrum fit
278 procedure at temperature T are then calculated as the square root of the quadratic sum of the type-
279 A and type-B errors. These 1σ -uncertainties are plotted in **Figure 3**. By looking at these plots, we see
280 no systematic difference between the experimental data points and the fitted curves. We also
281 observe that the estimated final uncertainties are consistent with the dispersion of the parameter
282 values, the fitted curves being within a $\pm 2\sigma$ interval in most of the cases. We nevertheless note that

283 the final uncertainties of the parameters at temperature T seem to be underestimated by a factor of
284 ~ 2 for the δ_0 , α_w and ζ parameters at 285 and 320 K for some transitions and for the β parameter of
285 the R(6) transition.

286 The uncertainties included in **Table 2** for the spectroscopic parameters at $T_{ref}= 296$ K and their
287 temperature dependence exponent, correspond to the fit error taking into account the uncertainties
288 on the spectroscopic parameters at each temperature. Quoted uncertainties values in Table 2 are
289 smaller than those presented in **Fig. 3** because they are based on five data points (or temperatures)
290 thus bringing more constraints on the fit.

291 **4. Discussion**

292 As mentioned above, a number of previous spectroscopic works have already been reported for
293 the $^{12}\text{CO}_2$ band studied here. We will limit our discussion to:

294 (i) The FTS measurements by Devi et al. [1] (also named hereafter Devi2016), whose results,
295 obtained with a quadratic speed-dependent Voigt profile including line-mixing, are implemented in
296 the latest version (5.1) of the absorption coefficient (ABSCO) tables for the Orbiting Carbon
297 Observatories for the 1.6 μm band [30],

298 (ii) The latest version of the HITRAN database (HITRAN2020) [18] which is based on empirical
299 modeling described in Ref. [20], adopting as in Ref. [1] a quadratic speed-dependent Voigt profile
300 with line-mixing,

301 (iii) The rCMDS calculations [21] (also named hereafter Nguyen2020) which provides Voigt
302 and non-Voigt line-shape parameters to complement the databases when no experimental data are
303 available. Note that the rCMDS spectroscopic parameters are only given for the P-branch, but
304 Nguyen et al. indicated that *the calculated R branch spectrum will be the exact symmetric of the P*
305 *branch* that we interpret as *the rCMDS spectroscopic parameters are function of the absolute value of*
306 *m where $m=-J$ and $J+1$ for the P- and R-branch, respectively* [21].

307 (iv) The Frequency-stabilized (FS)-CRDS measurements on the R(16) transition of the studied
308 band done at NIST between 240 and 290K using a SDNG profile (also named hereafter Ghysels2017)
309 [7].

310 Recently, several CRDS studies have reported highly accurate measurements (at the kHz level
311 or below) of the positions of the studied CO_2 transitions by saturation spectroscopy [6] or from
312 Doppler limited spectra [4,5]. The comparison of our fitted positions with the values provided by
313 these studies shows averaged differences (over the 5 transitions) from 25 kHz at 250K and 285 K, for
314 which the best signal-to-noise ratios are achieved, to 150 kHz in the worst case at 320 K. Fixing the
315 positions to these very accurate values during the multi-spectrum fit procedure modifies only
316 marginally the values retrieved for the different line-shape parameters.

317 a. *Comparison of the air-broadening coefficients and their temperature dependence*

318 Comparison of the retrieved air-broadening coefficients, $\gamma_0(T_{ref})$, with Devi et al, HITRAN and
319 rCMDS values is presented in the upper panel of **Figure 4**. As already observed in [20], rCMDS values
320 are systematically lower than measurements with differences of up to 2.6% compared to our values.
321 Let us remind, that in the rCMDS calculations, the molecules were considered as rigid rotors so that
322 all the effects of vibrational motion were disregarded. In fact, as shown in Fig. 6 of [31], the air-
323 broadening coefficients at 296 K increase with the vibrational excitation up to few percent's. Due to
324 the underestimation of the rCMDS values, HITRAN2020 adopted rCMDS values for the air-broadening
325 coefficients of CO₂ [20] after a rescaling according to the FTS values of Devi et al.. In the lower panel
326 of **Figure 4**, we present the ratios of the experimental air-broadening coefficients to the
327 corresponding HITRAN2020 values. The agreement of our values with HITRAN2020 values is within
328 the HITRAN error bars (*i.e.* 1%) with differences from $\sim 0.1\%$ for R(6) line to 0.85% for the R(16), R(18)
329 and R(20) lines. Interestingly, a systematic difference by about 0.5 % is noted between the P- and R-
330 branches for the FTS values of Devi et al. This difference is between one and two orders of
331 magnitude larger than the experimental error bars of Devi et al. The same behavior is observed for
332 the 30012-00001 band from the data reported in [32]. If confirmed, it would indicate that a universal
333 law in $|m|$, as adopted in the HITRAN list for the air-broadening coefficients, is not adequate to
334 accurately account for the rotational dependence of the air-broadening coefficient in CO₂.

335 Air-broadening coefficients obtained in this work in the R-branch and by Devi et al. are close to
336 each other (**Figure 4**) with differences from -0.18% for the R(18) transition to +0.39% for the R(6)
337 transition. Nevertheless, for this latter transition, the particular FTS value seems to be $\sim 0.3\%$ smaller
338 than what could be extrapolated from the higher J lines of the R branch.

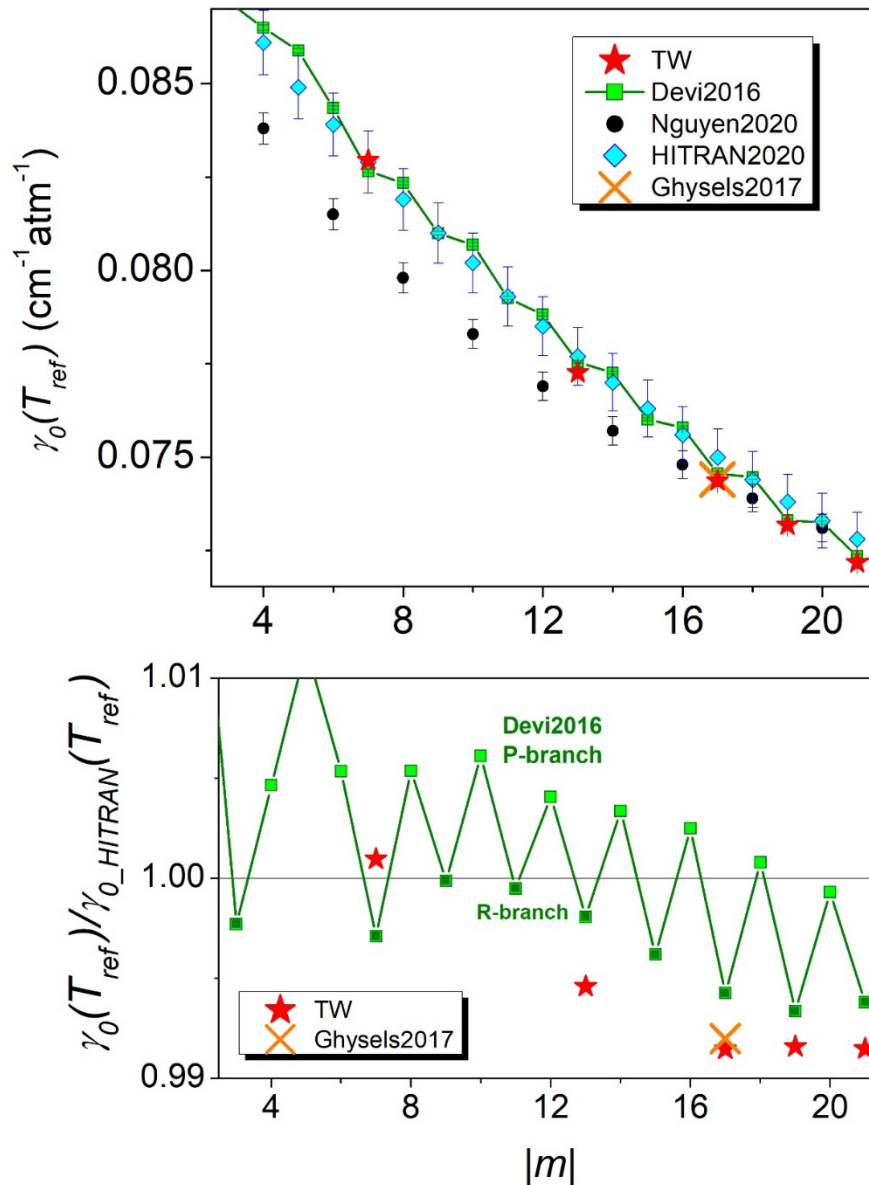
339 It is interesting to consider the impact of the line profile on the derived γ_0 values in particular
340 because Devi et al. adopted a SDV profile to model their FTS data while a SDNG profile was found
341 necessary to reproduce our CRDS spectra (see **Figure 2**). Following what has been done above to
342 quantify the temperature and pressure biases, we ran our fitting program with a SDV profile instead
343 of a SDNG profile. The γ_{0_SDV} fitted values were found systematically higher than our γ_{0_SDNG} values by
344 0.15 to 0.17%, thus compensating a significant part of the observed deviations (except for the R(6)
345 transition).

346 Another possible difference is related to the presence of argon in the air sample used for the
347 measurements. The dry air sample used by Devi et al corresponds to *Ultra Zero grade* from Airgas
348 which is a synthetic blend of 20-22% of oxygen and nitrogen, as found in the supplier documentation,
349 without 1% of argon contrary to our air sample. To evaluate the impact of argon, we used the results
350 of Ref. [32] where the O₂-, N₂- and Ar-broadening coefficients are measured for the nearby 30012-
351 00001 CO₂ band by frequency-agile rapid scanning (FARS) CRDS technique. Replacing 1% of N₂ by 1%
352 of Ar leads to a decrease of the broadening coefficient by $\sim 0.2\%$. Note that the exact O₂ mixing ratio

353 in the mixture used by Devi et al. is not given and could also have an effect on the reported
 354 broadening coefficients.

355 After correction of the FTS data from these two effects, the differences are reduced to less than
 356 0.2% for the R(10), R(16), R(18) and R(20) transitions, the deviation of the R(6) “outlier” reaching a
 357 value of 0.7%. This level of agreement fully satisfies the OCO-2/3 requirement of 0.6% for the width
 358 (Table 1 of Ref.[13]).

359



360

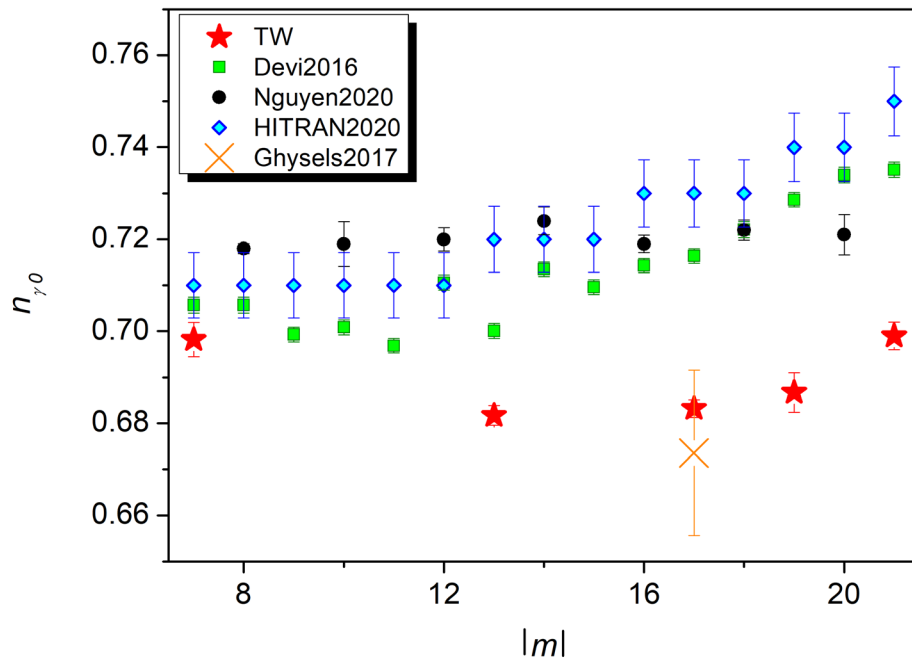
361

362 *Figure 4. Comparison of the retrieved air-broadening coefficients, $\gamma_0(T_{ref})$, with a selection of recent works:*
 363 *Devi2016 [1], Nguyen2020 [21], Ghysels2017 [7] and HITRAN2020 [18] (Upper panel). Ratios of the air-*
 364 *broadening coefficients obtained in this work (TW), in Devi2016 and in Ghysels2017 to those of HITRAN2020 are*

365 presented in the lower panel. A 1%-uncertainty is reported for HITRAN2020 values. Note the weak asymmetric
 366 behavior between the P- and R-branch.

367 We have included in Fig. 4, the NIST value for the R(16) transition [7] obtained for 400 ppm of CO₂
 368 in purified dry air (thus containing argon as in our sample) using a SDNG profile. An excellent
 369 agreement is achieved (difference of about 0.04%).

370 From this discussion, we conclude that accuracy on the γ_0 determination at the 0.1% level
 371 requires to carefully consider the impact of the line profile and the composition of the dry air sample
 372 (fraction of O₂ and N₂, presence of argon).

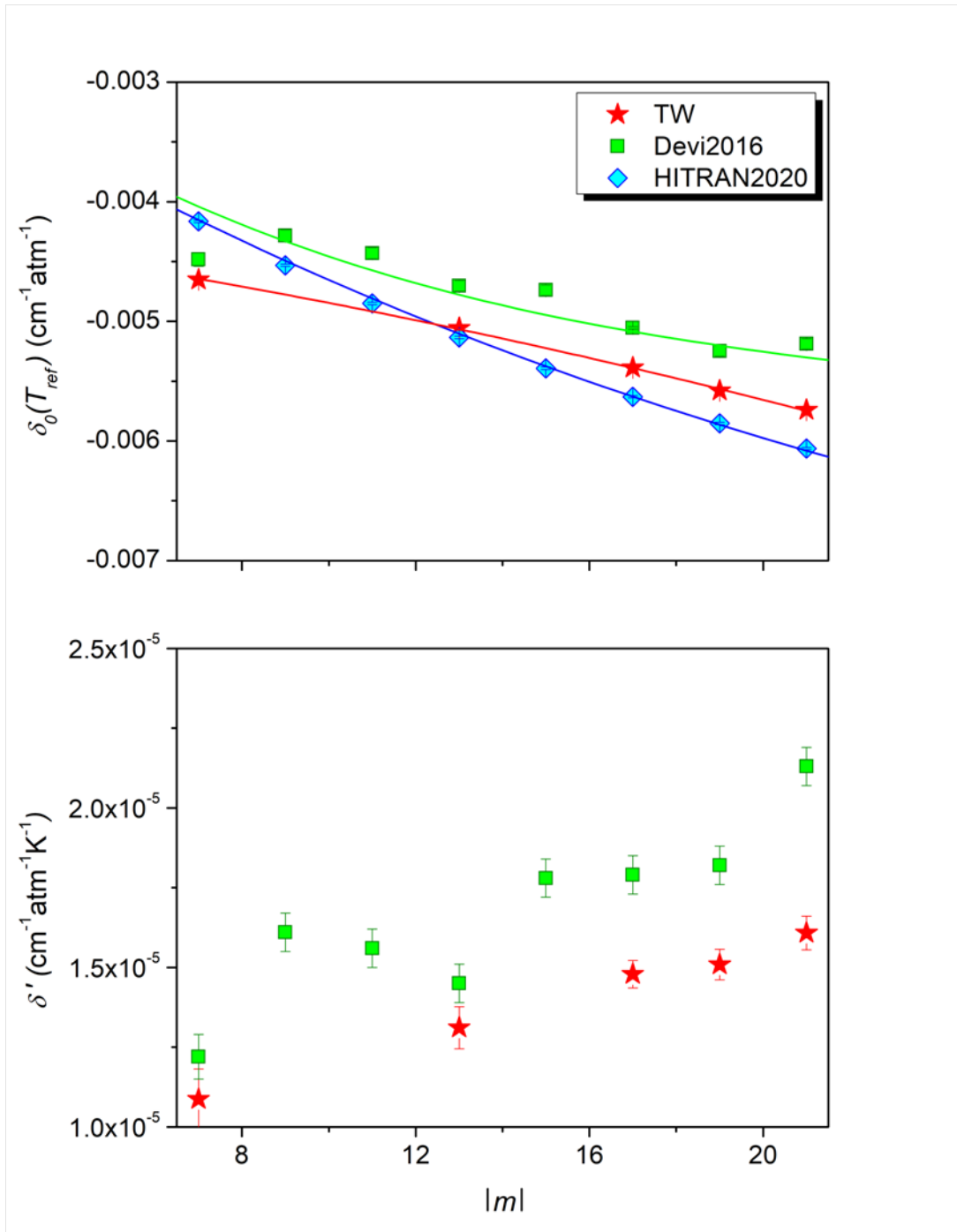


373
 374 *Figure 5. Comparison of the retrieved temperature dependence exponent of the air-broadening coefficient,*
 375 *n_{γ_0} , with a selection of recent works: Devi2016 [1], Nguyen2020 [21], Ghysels2017 [7] and HITRAN2020 [18].*

376 The γ_0 temperature dependence exponent obtained in the present work shows a clear m
 377 dependence contrary to the rCMDS calculated values which are almost constant for $|m| > 5$ (see **Fig.**
 378 **5**). The rCMDS values are systematically higher by 2.5 to 6% which can be considered as satisfactory
 379 for these calculations [21]. The comparison with Devi et al gives differences on the same order. As
 380 rCMDS calculations of n_{γ_0} for air and O₂ show that n_{γ_0} is not very sensitive to the perturber [21], the
 381 observed deviations cannot be due to the presence of 1% of argon in our air mixture. The observed
 382 differences are possibly explained by the use of different line profiles (*i.e.* SDNG profile in this work
 383 and a SDV profile in Devi et al.) and/or may be linked to temperature errors in the Devi et al
 384 measurements.

385 For the R(16) transition we see that the NIST n_{γ_0} value [7] obtained with a SDNG profile agrees
386 with our value. In the same paper, the n_{γ_0} value retrieved from a SDV profile was found in very good
387 agreement with the value reported in Devi et al. which might indicate that temperature dependence
388 exponent of the air-broadening coefficient is quite sensitive to the choice of the profile. The fitting of
389 our spectra with a SDV profile did not confirm this sensitivity, the retrieved n_{γ_0} value being almost
390 unchanged when using one or the other profile (including line-mixing effects). Note that NIST
391 estimated uncertainty of 0.018 is about ten times larger than what is estimated for the same
392 transition in our work (0.002). If we try to fit our $\gamma_0(T)$ data by fixing n_{γ_0} to the values reported by Devi
393 et al. (and by freeing $\gamma_0(T_{ref})$), a clear mismatch between the fit and our data is observed with
394 differences up to $\pm 0.4\%$ for the two “extreme” temperatures (250 and 320 K). This shows the
395 importance of an accurate determination of n_{γ_0} . As HITRAN2020 values are fitted on the FTS data of
396 Devi et al. with Padé approximants, similar differences are observed compared to HITRAN values.

397 *b. Comparison of the air-pressure shifts and their temperature dependence*



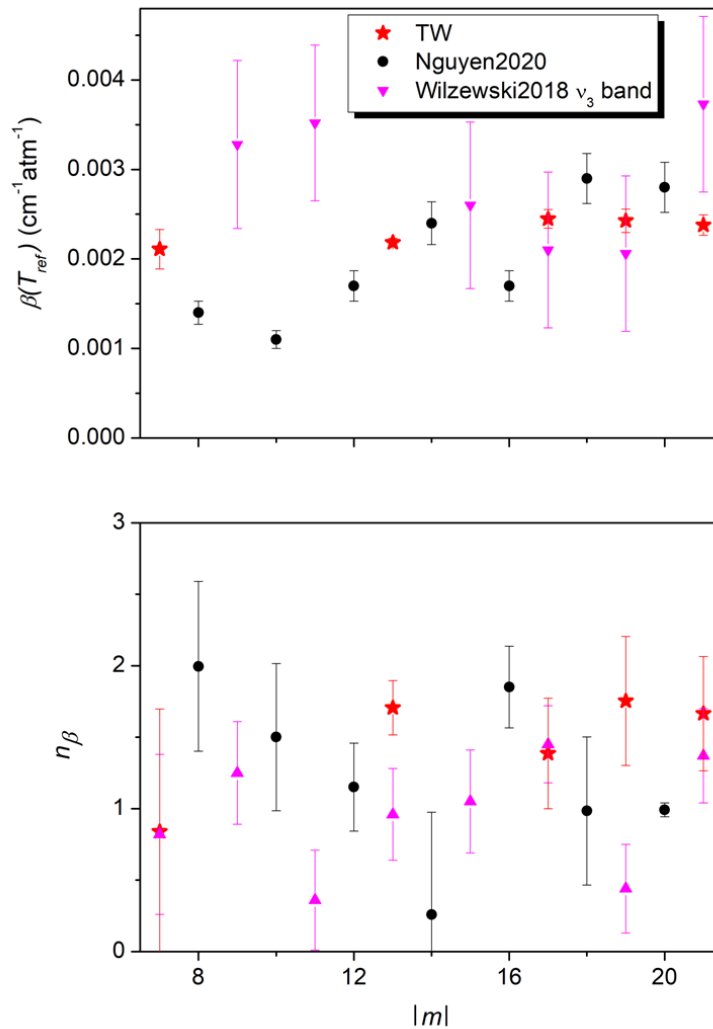
398

399 *Figure 6. Comparison of the retrieved air-pressure shift coefficients, $\delta_0(T_{ref})$, (Upper panel) and its*
 400 *temperature dependence coefficients, δ' , with Devi2016 [1] and HITRAN2020 [18]. Note that no temperature*
 401 *dependence is reported in HITRAN2020.*

402 In HITRAN2020, the approach proposed by Hartmann [33] is adopted to extend to other
 403 vibrational bands the air-pressure shift coefficients fitted to one band. The good agreement observed
 404 with our data (**Figure 6**) demonstrates the relevance of this approach. Devi et al. pressure shifts are
 405 smaller than our values by amounts between 3×10^{-4} and $5.5 \times 10^{-4} \text{ cm}^{-1} \text{atm}^{-1}$ which are outside the
 406 combined error bars. But, the reported FTS error bars (typ. $4.5 \times 10^{-5} \text{ cm}^{-1} \text{atm}^{-1}$) do not include

407 systematic uncertainties due to wavenumber calibration of the spectra and physical conditions of the
 408 spectra. Let us note here that the wavenumber calibration of the FTS spectra recorded by Devi et al
 409 was performed using additional absorption cells containing gases (CO, C₂H₂ or HCl) for which some
 410 transitions have accurately known positions, so that the overall FTS absolute uncertainty on line
 411 positions was estimated to be better than $\pm 0.0001 \text{ cm}^{-1}$. This uncertainty is a factor of 20 larger than
 412 the worst uncertainty on the absolute value of our fitted line positions. Our pressure-shift
 413 temperature dependence coefficients are close to the FTS values (although outside the combined
 414 error bars) and show an overall smooth increase with $|m|$ (lower panel of **Figure 6**).

415 *c. Comparison of the Dicke narrowing parameters*

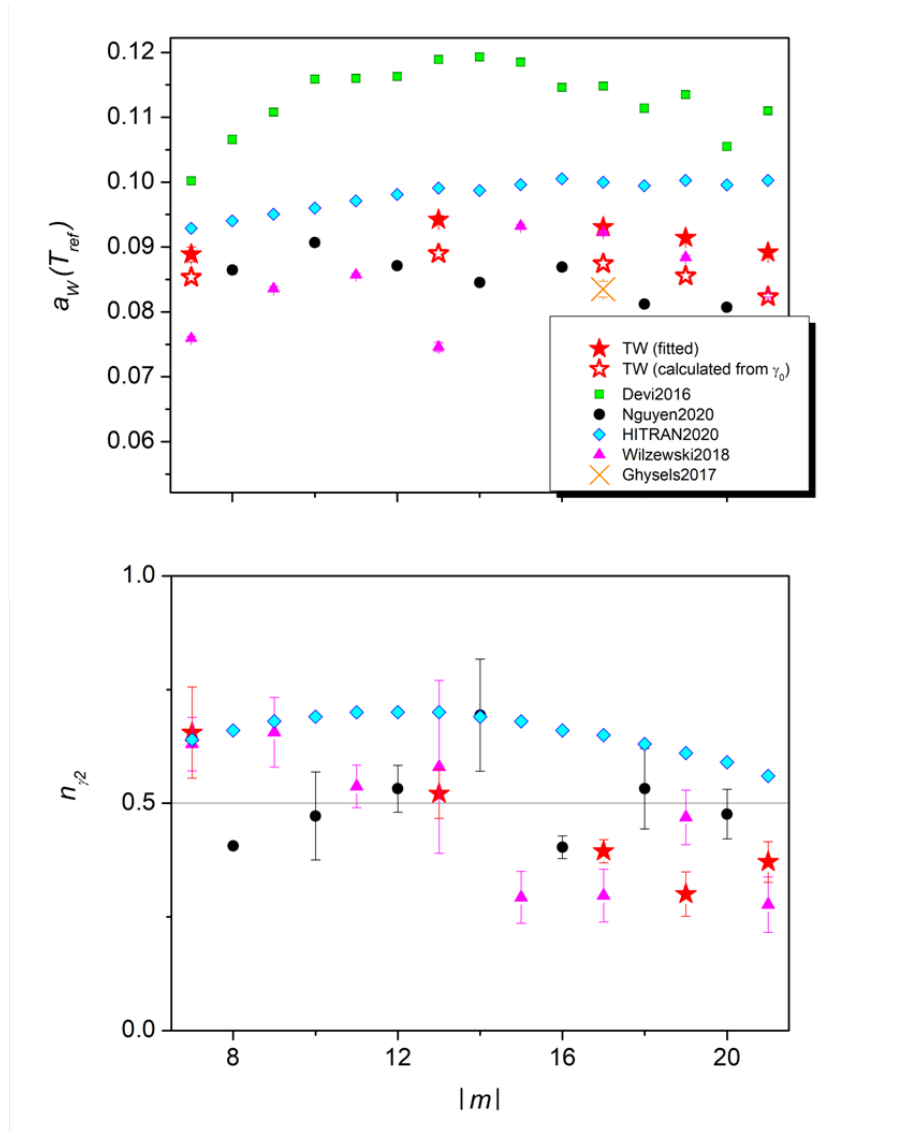


416
 417 *Figure 7. Comparison of the retrieved Dicke narrowing coefficients, $\beta(T_{ref})$, and of its temperature*
 418 *dependence exponent, n_β , with a selection of recent works: Nguyen2020 [21] and Wilzewski2018 [34].*

419 As expected, no evident m dependence is observed for β and n_β (**Figure 7**). With a weighted mean
 420 value over m of $0.00230(18) \text{ cm}^{-1}\text{atm}^{-1}$, our Dicke narrowing coefficients are found in good

421 agreement with SDNGP values obtained in Wilzewski2018 [34] for the ν_3 band of $^{12}\text{CO}_2$ in N_2 and with
 422 the rCMDS values [21] (for CO_2 in air). Note that these values are quite different from the value of
 423 $0.0199 \text{ cm}^{-1}\text{atm}^{-1}$ obtained from the diffusion coefficient of CO_2 in air derived from the kinetic theory
 424 of gases [29,35]. The retrieved temperature dependence exponents of the Dicke narrowing
 425 coefficients, n_β , are not accurately determined neither by experiment nor by rCMDS calculations
 426 (**Figure 7**) but the different values roughly agree within their large error bars. In our case, the
 427 weighted mean value of n_β is 1.45 ± 0.32 .

428 *d. The speed-dependent parameters and their temperature dependence*



429
 430 *Figure 8. Comparison of the speed dependent parameter, $a_w(T_{ref})$, and of its temperature dependence*
 431 *exponent, n_{γ_2} , with a selection of recent works: Devi2016 [1], Nguyen2020 [21], Ghysels2017 [7],*
 432 *Wilzewski2018 [34] and HITRAN2020 [18].*

433 The $|m|$ dependence of the speed dependent broadening parameter, $a_w(T_{ref})$, is presented in
 434 **Figure 8** together with selected literature data. According to Ref. [36], the $a_w(T_{ref})$ values can be

435 computed from the retrieved $\gamma_0(T)$ broadening coefficients and the m_p/m_a mass ratio where m_p and
436 m_a correspond to the mass of the perturber and of the absorber, respectively. The obtained values,
437 included in **Figure 8**, are found consistent with our $a_w(T_{ref})$ values although systematically smaller by
438 5-7%. Our values are also in good agreement with the rCMDS and HITRAN2020 data and the
439 experimental values of Wilzewski et al. [34] based on a quadratic SDNG profile. Note that the latter
440 study concerns the ν_3 band of CO_2 in N_2 and not in air. But, by using Ref. [36] to calculate $a_w(T)$, we
441 see that replacing air by N_2 decreases $a_w(T_{ref})$ by only 2% for the R(20) transition for example. The a_w
442 value reported by NIST for the R(16) transition is 11.5% lower than our value but this could be
443 explained by the fact that a_w was considered as independent of the temperature [7].

444 The FTS values of Devi et al. are notably larger than other experimental sources by about 25%.
445 This difference should only be partially explained by the use of a SDV profile instead of a SDNG
446 profile in our work. Indeed, simulations based on the MATS program, indicate that, in our conditions,
447 replacing the SDNG profile by a SDV one, leads to an increase of a_w by 5 to 6%. The agreement of
448 Devi et al. is also not very good with the HITRAN2020 data derived from rCMDS using a SDV profile.
449 The difference may also be related to the fact that Devi et al. assumed that a_w is identical for both
450 self- and air-broadening and independent of the gas sample temperature ($n_{\gamma_2} = 0$). This latter
451 assumption is in contradiction with both our results and the experimental results reported by
452 Wilzewski et al. for the ν_3 band (with n_{γ_2} on the order of 0.5) (**Figure 8**).

453 The rCMDS and HITRAN2020 n_{γ_2} values (derived from rCMDS calculations fitted with a SDV
454 profile) are in rough agreement with the experimental data. Note that our data and those of
455 Wilzewski et al. seem to show a slow decrease with $|m|$ contrary to rCMDS and HITRAN2020 data.

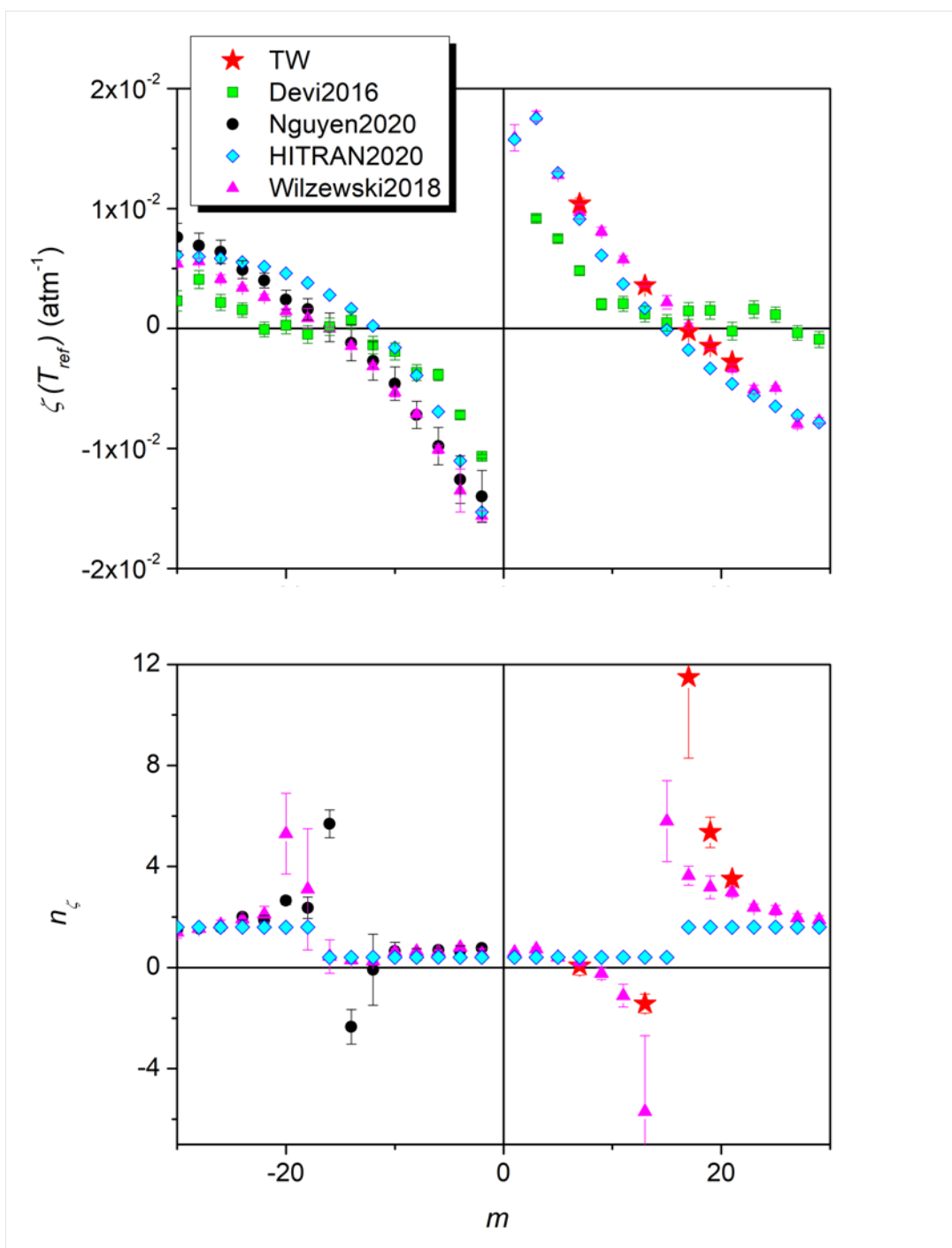
456 To our knowledge, no data are available for comparison of a_s (**Table 2**) for which no temperature
457 dependence is detected. A clear decrease with m from 0.093 to 0.053 for $m= 7$ to 21 is obtained for
458 the values averaged over the five temperatures of our measurements.

459 *e. The line-mixing parameters and their temperature dependence*

460 Our first-order line mixing parameters at 296 K are plotted on **Figure 9** together with the rCMDS,
461 HITRAN2020 values and the ν_3 results of [34]. The experimental values (relative to different bands)
462 are in close coincidence indicating that there is almost no vibrational dependence. This is confirmed
463 by the rCMDS results (with no vibrational dependence considered) which are systematically smaller
464 but agree satisfactorily with both experimental datasets. The same satisfactory agreement is
465 observed with HITRAN2020 values calculated by Lamouroux et al. [37] using the Energy-Corrected
466 Sudden (ECS) approximation.

467 Devi et al. reported off-diagonal relaxation matrix element coefficients, W_{ij} , between the nearest
468 neighbor pairs. Unfortunately, no explicit form of W_{ij} is given in Devi et al. So, to convert these matrix

469 element coefficients into the line-mixing parameters plotted on **Figure 9**, we adopted Eq. IV.24 of
 470 [28] and Eq. 7 of [38]. The m dependence derived in that way from Devi et al. differs noticeably from
 471 the experimental values. Devi et al mentioned that *the values of these line mixing temperature*
 472 *dependence exponents (...) showed no systematic variations with m or J contrary to what is shown on*
 473 **Figure 9**, where the CRDS, FTS and rCMDS temperature dependence exponents, n_ζ , are all in good
 474 agreement, showing a clear dependence with m with a rapid variation near $m=15$. To simplify the
 475 calculations with HAPI [39], two average values over m were adopted for in HITRAN2020 with $n_\zeta =$
 476 0.41 for $m \leq 16$ and $n_\zeta = 1.6$ for $m > 16$ [20].



477

478 *Figure 9. Comparison of the line-mixing parameter, $\zeta(T_{ref})$, and of its temperature dependence exponent, n_ζ ,*
479 *with a selection of recent works: Devi2016 [1], Nguyen2020 [21], Wilzewski2018 [34] and HITRAN2020 [18].*

480 **5. Conclusion**

481 Line-shapes of five transitions of the 30013-00001 band of carbon dioxide have been studied from
482 high sensitivity CRDS spectra recorded with the help of a narrowed and stable (sub-kHz) laser source.
483 Series of spectra were recorded in different conditions of temperature (from 250 to 320 K) and
484 pressure (from 50 to 750 Torr) for a mixture of ~ 400 ppm of CO_2 in air. From a multi-spectrum fit
485 procedure using quadratic SDNG profiles, including the line-mixing effects, the line-shape parameters
486 were retrieved with reduced uncertainties, meeting the most important requirements of the
487 demanding CO2M mission (i.e. on the air-broadening coefficients and their temperature
488 dependence), and limited numerical correlations. Temperature dependence is reported for all of
489 these parameters. Noticeably, contrary to what was claimed in some previous works, a clear
490 temperature dependence is noticed for the speed dependence component of the air-broadening
491 coefficient, very similar to what has been observed in Wilzewski et al. for the ν_3 band of CO_2 . No
492 temperature dependence is observed for the speed dependence component of the air pressure-shift
493 coefficient. A good overall agreement is obtained with rCMDS data for the different parameters,
494 which contributes to the validation of these calculations aiming to fill the databases for the non-Voigt
495 spectroscopic parameters.

496 A comparison with HITRAN2020 shows that the values reported in this database for the air
497 pressure-broadening and -shift coefficients of the studied transitions are in good agreements with
498 our values. An agreement better than 0.2% is found between the air-pressure-broadening
499 coefficients obtained at 296 K in this work and those from Devi et al., used in the ABSCO tables for
500 the OCO missions, for four of the five transitions studied. Nevertheless, the temperature dependence
501 exponents in Devi et al are systematically higher by up to 6% leading to differences close to 1% for γ_0
502 at the lowest atmospheric temperatures. Interestingly, the comparison of our results to the air
503 pressure-broadening available in the literature, in particular the FTS values of Devi et al. and the
504 CRDS values of Adkins et al. [32], revealed a systematic difference by about 0.5 % between the P- and
505 R- branches (**Fig. 4** bottom panel), largely above the experimental uncertainty. The origin of this
506 effect which was apparently not noted in Refs. [1,29], remains unclear but may indicate that the
507 universal law in $|m|$, as adopted in the HITRAN list for the air-broadening coefficients, is not
508 adequate to account for the rotational dependence of the air-broadening coefficient in CO_2 at the
509 level of accuracy achieved by the best experiments. Different empirical laws for the P- and R-
510 branches might be required.

511

512 **Acknowledgements**

513 This work is funded by the European Space Agency (ESA) through the contract No.
514 4000132228/20/I-NS with Deutsches Zentrum für Luft- und Raumfahrt) entitled *Improved*
515 *Spectroscopy for Carbon Dioxide, Oxygen, and Water Vapour Satellite Measurements* for which the
516 authors are sub-contractants. DM wants to thank H. Tran for fruitful discussions on rCMDS results.
517

- [1] Devi VM, Benner DC, Sung K, Brown LR, Crawford TJ, Miller CE, Drouin BJ, Payne VH, Yu S, Smith MAH, Mantz AW, Gamache RR. Line parameters including temperature dependences of self- and air-broadened line shapes of $^{12}\text{C}^{16}\text{O}_2$: 1.6- μm region. *J Quant Spectrosc Radiat Transf* 2016;177:117-144. Doi: 10.1016/j.jqsrt.2015.12.020.
- [2] Birk M, Röske C, Wagner G. High accuracy CO_2 Fourier transform measurements in the range 6000–7000 cm^{-1} . *J Quant Spectrosc Radiat Transf* 2021;272:107791. Doi: 10.1016/j.jqsrt.2021.107791.
- [3] Long DA, Truong G-W, Hodges JT, Miller CE. Absolute $^{12}\text{C}^{16}\text{O}_2$ transition frequencies at the kHz-level from 1.6 to 7.8 μm . *J Quant Spectrosc Radiat Transf* 2013;130:112-115. Doi : 10.1016/j.jqsrt.2013.07.001.
- [4] Reed ZD, Drouin BJ, Long DA, Hodges JT. Molecular transition frequencies of CO_2 near 1.6 μm with kHz-level uncertainties. *J Quant Spectrosc Radiat Transf* 2021; 271:107681. Doi : 10.1016/j.jqsrt.2021.107681.
- [5] Reed ZD, Drouin BJ, Hodges JT. Inclusion of the recoil shift in Doppler-broadened measurements of CO_2 transition frequencies. *J Quant Spectrosc Radiat Transf* 2021; 275:107885. Doi : 10.1016/j.jqsrt.2021.107885.
- [6] Wu H, Hu C-L, Wang J, Sun YR, Tan Y, Liu A-W, Hu S-M. A well-isolated vibrational state of CO_2 verified by near-infrared saturated spectroscopy with kHz accuracy. *Phys Chem Chem Phys* 2020;22:2841-2848. Doi: 10.1039/C9CP05121J
- [7] Ghysels M, Liu Q, Fleisher AJ, Hodges JT. A variable-temperature cavity ring-down spectrometer with application to line shape analysis of CO_2 spectra in the 1600 nm region. *Appl Phys B* 2017;123:124. Doi :10.1007/s00340-017-6686-y
- [8] Crisp D, Atlas RM, Breon F-M, Brown LR, Burrows JP, Ciais P, Connor BJ, Doney SC, Fung IY, Jacob DJ, Miller CE, O'Brien D, Pawson S, Randerson JT, Rayner P, Salawitch RJ, Sander SP, Sen B, Stephens GL, Tans PP, Toon GC, Wennberg PO, Wofsy SC, Yung YL, Kuang Z, Chudasama B, Sprague G, Weiss B, Pollock R, Kenyon D, Schroll S. The Orbiting Carbon Observatory (OCO) mission mission. *Adv Space Res* 2004;34:700–709. Doi: 10.1016/j.asr.2003.08.062.
- [9] Crisp D, Miller CE, DeCola PL. NASA Orbiting Carbon Observatory: measuring the column averaged carbon dioxide mole fraction from space. *J Appl Rem Sens* 2008;2:023508. Doi: 10.1117/ 1.2898457.
- [10] Boesch H, Baker D, Connor B, Crisp D, Miller CE. Global characterization of CO_2 column retrievals from shortwave-infrared satellite observations of the Orbiting Carbon Obs-2 Mission. *Remote Sens* 2011;3:270–304. Doi: 10.3390/rs3020270
- [11] Eldering A, Taylor TE, O'Dell CW, Pavlick R. The OCO-3 mission: measurement objectives and expected performance based on 1 year of simulated data. *Atmos Meas Tech* 2019;12:2341–2370. Doi: 10.5194/amt-12-2341-2019.
- [12] Kuze A, Suto H, Nakajima M, Hamazaki T. Thermal and near infrared sensor for carbon observation Fourier transform spectrometer on the Greenhouse Gases Observing Satellite for greenhouse gases monitoring. *Appl Opt* 2009;48:6716–33. Doi:10.1364/AO.48.006716.
- [13] Miller CE, Crisp D, DeCola PL, Olsen SC, Randerson JT, Michalak AM, Alkhaled A, Rayner P, Jacob DJ, Suntharalingam P, Jones DBA, Denning AS, Nicholls ME, Doney SC, Pawson S, Boesch H, Connor BJ, Fung IY, O'Brien D, Salawitch RJ, Sander SP, Sen B, Tans P, Toon GC, Wennberg PO, Wofsy SC, Yung YL, Law RM. Precision requirements for space-based X_{CO_2} data. *J Geophys Res: Atmos* 2007;112:D10314. Doi:10.1029/2006JD007659
- [14] Hobbs JM, Drouin BJ, Oyafuso F, Payne VH, Gunson MR, McDuffie J, Mlawer EJ. Spectroscopic uncertainty impacts on OCO-2/3 retrievals of X_{CO_2} . *J Quant Spectrosc Radiat Transf* 2020;257:107360. Doi: 10.1016/j.jqsrt.2020.107360.
- [15] Copernicus CO_2 Monitoring Mission Requirements Document, EOP-SM/3088/YM-ymIssue 2.0, 2019. available via https://esamultimedia.esa.int/docs/EarthObservation/CO2M_MRD_v2.0_Issued20190927.pdf
- [16] ISOGG project TechNote WP2100: End user requirements for relevant satellite instruments.
- [17] ISOGG project TechNote: WP2200: Retrieval simulations.
- [18] Gordon IE, Rothman LS, Hargreaves RJ, Hashemi R, Karlovets EV, Skinner FM, Conway EK, Hill C, Kochanov RV, Tan Y, Wcisło P, Finenko AA, Nelson K, Bernath PF, Birk M, Boudon V, Campargue A, Chance KV, Coustenis A, Drouin BJ, Flaud J-M, Gamache RR, Hodges JT, Jacquemart D, Mlawer EJ, Nikitin AV, Perevalov VI, Rotger M, Tennyson J, Toon GC, Tran H, Tyuterev VG, Adkins EM, Baker A, Barbe A, Canè E, Császár AG, Dudaryonok A, Egorov O, Fleisher AJ, Fleurbaey H, Foltynowicz A, Furtenbacher T, Harrison JJ, Hartmann J-M, Horneman V-M, Huang X, Karman T, Karns J, Kassi S, Kleiner I, Kofman V, Kwabia-Tchana F, Lavrentieva NN, Lee TJ, Long DA, Lukashchanskaya AA, Lyulin OM, Makhnev VY, Matt W, Massie ST, Melosso M, Mikhailenko SN, Mondelain D, Müller HSP, Naumenko OV, Perrin A, Polyansky OL, Raddaoui E, Raston PL, Reed ZD, Rey M, Richard C, Tóbiás R,

-
- Sadiek I, Schwenke DW, Starikova E, Sung K, Tamassia F, Tashkun SA, Vander Auwera J, Vasilenko IA, Vigasin AA, Villanueva GL, Vispoel B, Wagner G, Yachmenev A, Yurchenko SN. The HITRAN2020 molecular spectroscopic database. *J Quant Spectrosc Radiat Transf* 2022; 277:107949. Doi: 10.1016/j.jqsrt.2021.107949.
- [19] Jacquinet-Husson N, Armante R, Scott NA, Chédin A, Crépeau L, Boutammine C, Bouhdaoui A, Crevoisier C, Capelle V, Boone C, Poulet-Crovisier N, Barbe A, Benner DC, Boudon V, Brown LR, Buldyreva J, Campargue A, Coudert LH, Devi VM, Down MJ, Drouin BJ, Fayt A, Fittschen C, Flaud J-M, Gamache RR, Harrison JJ, Hill C, Hodnebrog Ø, Hu S-M, Jacquemart D, Jolly A, Jiménez E, Lavrentieva NN, Liu A-W, Lodi L, Lyulin OM, Massie ST, Mikhailenko S, Müller HSP, Naumenko OV, Nikitin A, Nielsen CJ, Orphal J, Perevalov VI, Perrin A, Polovtseva E, Predoi-Cross A, Rotger M, Ruth AA, Yu SS, Sung K, Tashkun SA, Tennyson J, Tyuterev VG, Vander Auwera J, Voronin BA, Makie A. The 2015 edition of the GEISA spectroscopic database, *J Mol Spectr* 2016; 327:31-72. Doi : 10.1016/j.jms.2016.06.007.
- [20] Hashemi R, Gordon IE, Tran H, Kochanov RV, Karlovets EV, Tan Y, Lamouroux J, Ngo NH, Rothman LS. Revising the line-shape parameters for air- and self broadened CO₂ lines toward a sub-percent accuracy level, *J Quant Spectrosc Radiat Transf* 2020;256:107283. Doi: 10.1016/j.jqsrt.2020.107283.
- [21] Nguyen HT, Ngo NH, Tran H. Line-shape parameters and their temperature dependences predicted from molecular dynamics simulations for O₂- and air-broadened CO₂ lines. *J Quant Spectrosc Radiat Transf* 2020;242:106729. Doi: 10.1016/j.jqsrt.2019.106729.
- [22] Vasilchenko S, Delahaye T, Kassi S, Campargue A, Tran H, Mondelain D. Temperature dependence of the absorption of the R(6) manifold of the 2v₃ band of methane in air for the MERLIN mission. To be submitted to *JQSRT*.
- [23] Burkart J, Romanini D, Kassi S. Optical feedback stabilized laser tuned by single-sideband modulation. *Opt Lett* 2013;38:2062-2064. Doi:
- [24] Kassi S, Guessoum S, Abanto JCA, Tran H, Campargue A, Mondelain D. Temperature dependence of the collision-induced absorption band of O₂ near 1.27 μm. *J Geophys Res Atm* 2021;126:e2021JD034860. Doi : 10.1029/2021JD034860.
- [25] <https://github.com/usnistgov/MATS>. Doi:10.18434/M32200
- [26] Tran H, Ngo NH, Hartmann J-M. Efficient computation of some speed-dependent isolated line profiles. *J Quant Spectrosc Radiat Transf* 2013;129:199-20. Doi :10.1016/j.jqsrt.2013.06.015.
- [27] Rosenkranz PK. Shape of the 5 μm oxygen band in the atmosphere. *IEEE Trans Antennas Propag* 1975;23:498–506.
- [28] Hartmann J-M, Boulet C, Robert D, Chapter IV - Collisional line mixing (within clusters of lines), Editor(s): J-M Hartmann, C Boulet, D Robert, *Collisional Effects on Molecular Spectra (Second Edition)*, Elsevier, 2021, Pages 181-289. Doi : 10.1016/B978-0-12-822364-2.00004-0.
- [29] Adkins EM, Hodges JT. Assessment of the precision, bias and numerical correlation of fitted parameters obtained by multi-spectrum fits of the Hartmann-Tran line profile to simulated absorption spectra, *J Quant Spectrosc Radiat Transf* 2022;280:108100. Doi: 10.1016/j.jqsrt.2022.108100.
- [30] Payne VH, Drouin BJ, Oyafuso F, Kuai L, Fisher BM, Sung K, Nemchick D, Crawford TJ, Smyth M, Crisp D, Adkins E, Hodges JT, Long DA, Mlawer EJ, Merrelli A, Lunny E, O'Dell CW. Absorption coefficient (ABSCO) tables for the Orbiting Carbon Observatories: Version 5.1. *J Quant Spectrosc Radiat Transf* 2020;255:107217. Doi : 10.1016/j.jqsrt.2020.107217.
- [31] Gamache RR, Lamouroux J. The vibrational dependence of half-widths of CO₂ transitions broadened by N₂, O₂, air, and CO₂. *J Quant Spectrosc Radiat Transf* 2013;117:93-103. Doi: 10.1016/j.jqsrt.2012.10.028.
- [32] Adkins EM, Long DA, Hodges JT. Air-broadening in near-infrared carbon dioxide line shapes: Quantifying contributions from O₂, N₂, and Ar. *J Quant Spectrosc Radiat Transf* 2021;270:107669. Doi: 10.1016/j.jqsrt.2021.107669.
- [33] Hartmann J-M. A simple empirical model for the collisional spectral shift of air-broadened CO₂ lines. *J Quant Spectrosc Radiat Transfer* 2009;110(18):2019–2026. Doi:10.1016/j.jqsrt.2009.05.016
- [34] Wilzewski JS, Birk M, Loos J, Wagner G. Temperature-dependence laws of absorption line shape parameters of the CO₂ v₃ band. *J Quant Spectrosc Radiat Transf* 2018;206:296-305. Doi: 10.1016/j.jqsrt.2017.11.021.
- [35] <https://demonstrations.wolfram.com/BinaryDiffusionCoefficientsForGases/>
- [36] Lisak D, Cygan A, Wcislo P, Ciuryło R. Quadratic speed dependence of collisional broadening and shifting for atmospheric applications. *J Quant Spectrosc Radiat Transf* 2015; 151:43-48. Doi : 10.1016/j.jqsrt.2014.08.016.

-
- [37] Lamouroux J, Régalia L, Thomas X, Auwera JV, Gamache R, Hartmann J-M. CO₂ line-mixing database and software update and its tests in the 2.1 μm and 4.3 μm regions. *J Quant Spectrosc Radiat Transfer* 2015;151:88–96. Doi:10.1016/j.jqsrt.2014.09.017.
- [38] Tran H, Flaud J-M, Gabard T, Hase F, von Clarmann T, Camy-Peyret C, Payan S, Hartmann J-M. Model, software and database for line-mixing effects in the ν_3 and ν_4 bands of CH₄ and tests using laboratory and planetary measurements—I: N₂ (and air) broadenings and the earth atmosphere. *J Quant Spectrosc Radiat Transf* 2006;101:284-305. Doi: 10.1016/j.jqsrt.2005.11.020.
- [39] Kochanov RV, Gordon IE, Rothman LS, Wcislo P, Hill C, Wilzewski JS. HITRAN Application Programming Interface (HAPI): A comprehensive approach to working with spectroscopic data *J Quant Spectrosc Radiat Transfer* 2016;177:15-30. Doi : 10.1016/j.jqsrt.2016.03.005